Spherical Crystallization of Glycine from Monodisperse Microfluidic Emulsions

ARTICLE *in* CRYSTAL GROWTH & DESIGN · JULY 2012

Impact Factor: 4.89 · DOI: 10.1021/cg300413s

CRYSTAL GROWTH & DESIGN

Article

pubs.acs.org/crystal

Spherical Crystallization of Glycine from Monodisperse Microfluidic Emulsions

Arpad I. Toldy,[†] Abu Zayed M. Badruddoza,[‡] Lu Zheng,[‡] T. Alan Hatton,[†,§] Rudiyanto Gunawan,[∥] Raj Rajagopalan,[†,‡] and Saif A. Khan*[,†,‡]

[†]Chemical and Pharmaceutical Engineering Program, Singapore-MIT Alliance, 4 Engineering Drive 3, E4-04-10, Singapore 117576, Singapore

[‡]Department of Chemical and Biomolecular Engineering, National University of Singapore, 4 Engineering Drive 4, Singapore 117576, Singapore

[§]Department of Chemical Engineering, Massachusetts Institute of Technology, 77 Massachusetts Avenue, E19-520b, Cambridge Massachusetts 02139, United States

[∥]Institute for Chemical and Bioengineering, HCI F 101, Wolfgang-Pauli-Strasse 10, ETH Zurich, Switzerland, CH-8093

Supporting Information

ABSTRACT: Emulsion-based crystallization to produce spherical crystalline agglomerates (SAs) is an attractive route to control crystal size during downstream processing of active pharmaceutical ingredients (APIs). However, conventional methods of emulsification in stirred vessels pose several problems that limit the utility of emulsion-based crystallization. In this paper, we use capillary microfluidics to generate monodisperse water-in-oil emulsions. Capillary microfluidics, in conjunction with evaporative crystallization on a flat heated surface, enables controllable production of uniformly sized SAs of glycine in the 35−150 μm size range. We report detailed characterization of particle size, size distribution, structure, and polymorphic form. Further, online high-speed stereomicroscopic observations reveal several clearly demarcated stages in the dynamics of glycine crystallization from emulsion droplets. Rapid droplet shrinkage is followed by crystal nucleation within individual droplets. Once a nucleus is formed within a droplet, crystal growth is very rapid (<0.1 s) and occurs linearly along radially advancing fronts at speeds of up to 1 mm/s, similar to spherulitic crystal growth from impure melts. The spherulitic aggregate thus formed ages to yield the final SA morphology. Overall crystallization times are on the order of minutes, as compared to hours in conventional batch processes. We discuss these phenomena and their implications for the development of more generalized processes applicable to a variety of drug molecules. This work paves the way for microfluidics-enabled continuous spherical crystallization processes.

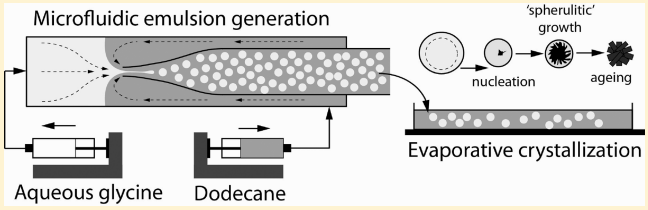

INTRODUCTION

Crystallization is one of the most important steps in the downstream processing of active pharmaceutical ingredients (APIs), and it is crucial to obtain crystals of the desired polymorphic form and size distribution in this processing step.[1] Emulsion-based crystallization of APIs, pioneered by Kawashima and co-workers,[2] wherein API crystals are generated within dispersed droplets in an immiscible continuous phase, is a promising method to produce API crystal agglomerates of controlled size. This approach leads to a particle size distribution corresponding to the droplet size distribution, provided that the conditions for crystallization are properly chosen.[3] The spherical agglomerates (SAs) thus produced have improved downstream processability (e.g., flowability, compressibility, compactibility)[4] and enhanced bioavailability due to the small size of the individual crystals that make up the SAs.[2] However, the conventional method of producing emulsions in stirred batch crystallizers leads to highly polydisperse emulsions (and therefore crystals) that severely limit the utility and general applicability of emulsion-based crystallization.

Droplet microfluidics, employing either microfabricated devices or concentric capillary tubes, is now an established method to produce highly monodisperse emulsions with exquisite control over droplet size.[5] The use of capillary-based droplet microfluidics for the fabrication of functional microparticles has been extensively demonstrated.[6] For example, controlled fabrication of polymeric particles,[7] smart polymerosomes,[8] and Janus particles[9] has been demonstrated. Another key application of droplet microfluidics has been in the area of high-throughput screening of crystal nucleation and growth conditions.[10−12] Several excellent studies have demonstrated the versatility of this platform in conducting rapid scans of protein crystallization parameter spaces, and even detailed

Received: March 28, 2012
Revised: June 14, 2012
Published: July 2, 2012

   dx.doi.org/10.1021/cg300413s | *Cryst. Growth Des.* 2012, 12, 3977−3982

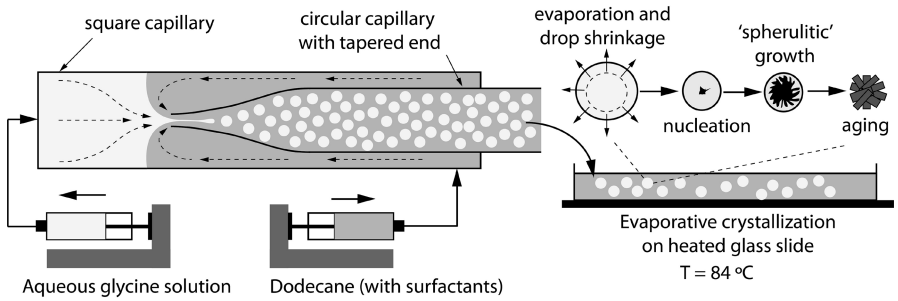

Figure 1. Schematic of experimental setup. Emulsion generation is performed in a concentric microfluidic glass capillary setup, where a square capillary (ID = 1 mm) houses a tapered round capillary (OD = 1 mm). The two ends of the square capillary function as inlets and the round capillary functions as a collection tube and outlet. The continuous phase (CP) of dodecane (with dissolved surfactants) and a dispersed phase (DP) of aqueous glycine are infused by syringe pumps into the square capillary. The emulsions are collected on a heated glass slide, where evaporative crystallization occurs. A more detailed description of the fabrication and assembly of the devices used is provided in the Supporting Information.

studies of the kinetics of crystal nucleation and growth.[13−15] Moreover, the use of microfluidics for studying the crystallization behavior of small organic molecules has also been demonstrated for both water[16] and organic-soluble molecules.[17] However, apart from high-throughput screening applications, microfluidic droplet generation for direct and scalable production of monodisperse spherical agglomerates of API crystals is a relatively unexplored area with much potential. Previous efforts to use microfluidics for the production of API crystals have mostly focused on spraying methods, which inherently produce nanoparticles[18] or a wide range of particle sizes.[19] Steinbacher and co-workers presented one of the first demonstrations of crystalline solids production with capillary microfluidics, by synthesizing core−shell organosilicon particles with a highly ordered internal structure.[20]

In this paper we present a microfluidics-based crystallization method consisting of a capillary microfluidic emulsion generator (based on the pioneering studies of Weitz and co-workers[21]) connected to a heated platform for evaporative crystallization, to produce spherical crystal agglomerates of glycine, an amino-acid often used as a model molecule for API crystallization studies, with tightly controlled size distributions over a fairly broad range of industrially relevant particle sizes. We report detailed characterization of SA particle size, size distribution, structure, and polymorphic form. Further, online high-speed stereomicroscopic observations reveal several clearly demarcated stages in the dynamics of glycine crystallization from emulsion droplets. Rapid droplet shrinkage is followed by nucleation within the emulsion droplets. Once a nucleus is formed within a droplet, crystal growth is very rapid (<0.1 s) and occurs linearly along radially advancing fronts at speeds of up to 1 mm/s, similar to spherulitic crystal growth from impure melts. The spherulitic aggregate thus formed ages to yield the final SA morphology. Overall crystallization times are on the order of minutes, as compared to hours in conventional batch processes. We discuss these phenomena and their implications for the development of more generalized processes applicable to a variety of drug molecules. Our work paves the way for microfluidics-enabled continuous spherical crystallization processes.

■ EXPERIMENTAL SECTION

Glycine (>99%), dodecane (>99%), Span-20, Span-80, and trichloro-(1*H*,1*H*,2*H*,2*H*-perfluorooctyl)-silane (97%) were purchased from Sigma-Aldrich and used as received. Ultrapure water (18.3 MΩ) obtained using a Millipore Milli-Q purification system was used to prepare aqueous glycine solutions. Sterile syringes (3 and 10 mL) and sterile single use needles (21 G 1 1/2") were purchased from Terumo Corporation, Japan. Syringe filters (0.45 μm) were purchased from Cole-Parmer. Microscope slides (Corning 75 × 50 mm) were used as a crystallization platform and for sample collection.

A schematic of our experimental setup and procedure is provided in Figure 1. Monodisperse emulsions were produced in a coaxial capillary setup, in which a round capillary (1 mm outer diameter) with a tapered end functions as a collection tube and the two immiscible liquids are infused through a coaxial outer square capillary (1 mm inner side).[21] We used two devices with different end diameters of the tapered round capillary — "narrow": 90 μm and "wide": 450 μm — to generate droplets within two broadly different size ranges. Dodecane was used as a continuous phase (CP) with a 2% (w/w) surfactant mixture consisting of 70% Span-20 and 30% Span-80 (w/w). The dispersed phase (DP) was a glycine solution saturated at room temperature (22 °C); therefore the glycine content was approximately 24.4 g of glycine/100 g of water.[22] This solution was filtered through a 0.45 μm syringe filter before each experiment. As shown in Figure 1, the glycine solution and dodecane−surfactant mixture were loaded into separate syringes and infused into the capillary emulsion generator using syringe pumps (Harvard PHD 22/2000 series) at various flow rates. The emulsions generated were directly dispensed for 10 s onto glass slides placed on a hot plate (Thermo Scientific CIMAREC) set to 90 °C. The surface temperature of the glass slides was measured with a thermometer (Lutron TM-914C) to be ∼84 °C. High-speed imaging of the droplet breakup and crystallization was performed with high-speed digital cameras (Basler pI640 or Miro Phantom EX2) mounted onto a stereomicroscope (Leica MZ16). An Olympus LG-PS2 light source with a gooseneck was used for illumination.

The SAs obtained were characterized in three different ways: microscopic image analysis for size distribution studies, field emission scanning electron microscopy (FE-SEM) for structural characterization, and powder X-ray diffraction (PXRD) for polymorphic characterization. For the size distribution studies we used an inverted microscope (Nikon Eclipse Ti) operated in dark field mode. The inbuilt software (NIS Elements 3.22.0) was used to measure the diameter of the agglomerates (circle by three points method) and to estimate the average diameters and standard deviations based on measurements of at least 100 SAs. A field-emission scanning electron microscope (JEOL JSM-6700F) at 5 kV accelerating voltage was used to acquire further structural information on the SAs. All samples were prepared on conventional SEM stubs with carbon tape and were coated with ∼10 nm of platinum by sputter coating. An XRD diffractometer (LabX XRD-6000, Shimadzu) with characteristic Cu radiation was used for polymorphic characterization. The crystal samples were ground into a fine powder and filled into the cavity of an aluminum sample holder that was mounted to a motorized stage for sample scanning. The X-ray diffractometer was operated at 40 kV, 30 mA and at a scanning rate of 2°/min over the range of 2θ = 10−40°, using the Cu radiation wavelength of 1.54 Å.

dx.doi.org/10.1021/cg300413s | *Cryst. Growth Des.* 2012, 12, 3977−3982

RESULTS AND DISCUSSION

Emulsion Generation. We used two different end taper sizes for the circular capillary in the emulsion generator (Figure 1), to produce broadly two size ranges of aqueous emulsion droplets that we classify as "large" (d = 200−320 μm range) and "small" (d = 70−120 μm range). By choosing appropriate combinations of oil and water volumetric flow rates (as indicated in Table 1), we were able to dispense droplets with tightly controlled sizes and distributions in the above ranges. Typical standard deviations for the emulsion droplets were <1% in all cases, highlighting the efficacy of the capillary microfluidic method in generating highly monodisperse water-in-oil emulsions.

Table 1. Summary of the Experimental Conditions and Droplets and Agglomerate Sizes Obtained under Different Conditions[a]

condition	device	Q_{CP} (μL/min)	Q_{DP} (μL/min)	D_D (μm)	D_A (μm)	std dev (%)
a	narrow	100	20	80	38	9
b	narrow	100	30	115	48	3
c	wide	1000	20	210	86	7
d	wide	1000	40	310	149	6

[a]Condition: as seen in Figures 3 and 4; Q_{CP}: flow rate of continuous phase; Q_{DP}: flow rate of dispersed phase; D_D: droplet diameter (with a standard deviation of less than 1% in all cases); D_A: average agglomerate diameter; std dev: standard deviation of agglomerate diameters.

Crystallization and Agglomerate Characterization. The emulsions generated were dispensed onto a heated glass slide maintained at 84 °C via a short length of tubing, where they formed a thin film of ∼0.2−0.5 mm depth. The following sequence of phenomena were observed to occur in each dispensed droplet: (1) rapid (i.e., within ∼10 s) shrinkage by ∼50% of the dispensed diameter in all cases, (2) onset of nucleation, with nucleation times varying from ∼10−300 s, (3) very rapid (<0.1 s) growth of the nucleus along radially advancing fronts that eventually stopped at the droplet boundary, and (4) aging of the crystal-filled droplet to yield spherical agglomerates (SAs). These individual stages will be discussed in further detail in Section III (crystallization dynamics) below.

A collection of microscopic images (under dark-field illumination) of SAs obtained under different conditions, histograms of particle sizes from the four samples, and a comparison of droplet and SA sizes are provided in Figure 2. The smooth size distribution of SAs obtained by this method is much narrower than that of comparable SAs produced by batch crystallization,[3] the most striking difference being the complete absence of extremely small or large SAs. For all sizes shown here, the diameter of SAs obtained is ∼50% of the original droplet diameter. Similar observations regarding droplet and SA diameters were reported by Chadwick et al. for the batch case.[3] Sphericity of the agglomerates was confirmed by field-emission scanning electron microscopy (FESEM) observations with a tilted stage (Figure 3). We observed that the size of the individual crystals that constitute the SAs increases as the size of the SAs increases. Larger SAs (>100 μm) were also more susceptible to breakage and flattening during handling and characterization, suggesting a balance between the structural

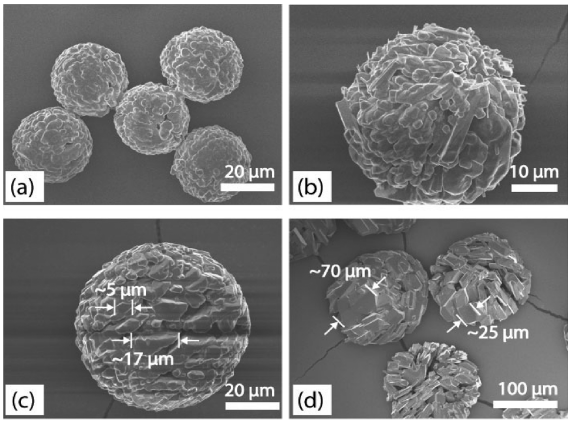

Figure 3. FE-SEM images of SAs obtained under different conditions (Table 1 and Figure 2). Smaller SAs [(a) and (b)] are comprised of compactly packed crystals of small (<10 μm) size, while larger SAs [(c) and (d)] consist of larger and, for the latter case, loosely packed crystals.

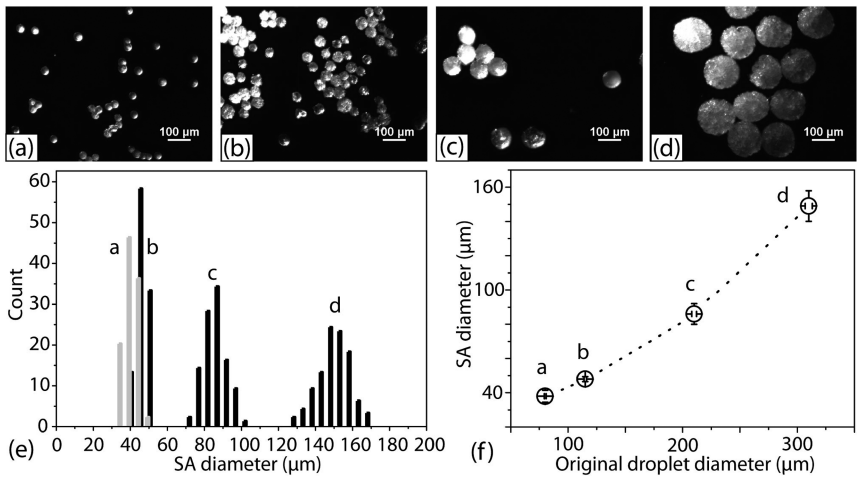

Figure 2. (a−d) Dark-field microscopy images of spherical agglomerates obtained under different conditions, (e) SA size distribution histograms for these samples (key parameters are summarized in Table 1), and (f) comparison of the dispensed droplet diameters with the average SA sizes obtained; droplets shrink to at least 50% of their original size before crystallization initiates.

dx.doi.org/10.1021/cg300413s | Cryst. Growth Des. 2012, 12, 3977−3982

integrity and the size of the SAs obtained, which has to be controlled by optimizing crystallization parameters (such as droplet size and the rate of supersaturation-generation). Finally, XRD results confirmed that the SAs we obtained were composed of predominantly the α polymorphic form under all conditions (a sample XRD pattern is provided in Figure 4;

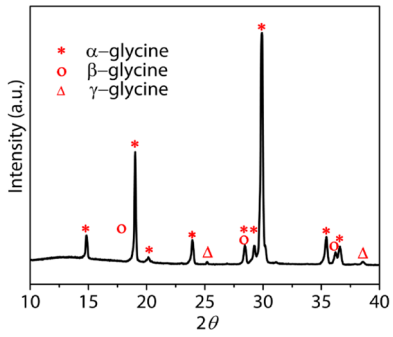

Figure 4. XRD characterization of SAs obtained from condition (d) (Table 1). Characteristic peak positions of all three polymorphs are indicated; the α polymorphic form is the dominant component.

α-glycine has characteristic peaks at 2θ values of 15, 19, 24, and 29.8°[23]); the β and γ forms were present only in minute amounts. We note that this is the expected result when crystallizing glycine from an aqueous solution.[22]

Crystallization Dynamics. Stereomicroscopic observations shed light on the various stages of crystallization. The dispensed emulsions started crystallizing on the heated slide after a short induction time (~10–40 s) in all cases, with a typical ensemble crystallization time of a few minutes. This overall crystallization time is significantly less than that observed in batch processes (typically on the order of hours).[3] As mentioned briefly in Section II above, the droplets first shrank rapidly as water evaporated through thin films of oil surrounding the droplets on the slide, following which nucleation occurred within the individual droplets. We conducted time-resolved droplet shrinkage and nucleation statistics measurements (sample results provided in Figure 5) and make the following comments on these phenomena.

First, it can be seen that droplets underwent rapid initial shrinkage following which the size remained essentially constant; the onset of nucleation/crystallization occurred during this latter phase. Shrinkage was complete within ~5 s while the earliest nucleation event occurred at ~25 s, implying that nucleation events could essentially be decoupled from shrinkage. Next, online nucleation induction time measurements were conducted on ensembles of droplets via direct microscopic observation, with ensemble sizes varying from 50 to 200; a typical histogram of measured nucleation events is superimposed in Figure 5a. Figure 5b shows a plot of the logarithm of probability of observing *no* nucleation event in a given drop versus time t and reveals an interesting feature of nucleation in our system. If nucleation in our system were a simple homogeneous Poisson process ($P(t) = \exp[(-t/\tau)]$, with a constant rate parameter $\lambda = 1/\tau$), the plot in Figure 5b would be linear. However, we observe a clear deviation from linearity and, remarkably, find that a compressed exponential model $-P(t) = \exp[(-t/\tau)^{\beta}]$, with time constant $\tau \sim 102$ s and compressed exponent $\beta \sim 2$, fits our data most satisfactorily. The compressed exponential model reflects a *nonhomogeneous*

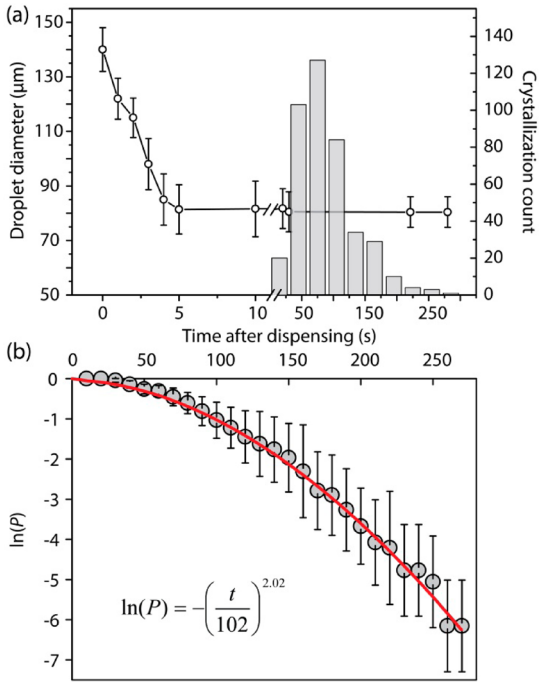

Figure 5. (a) Plot of droplet size versus time indicating shrinkage dynamics, with an overlaid histogram of nucleation statistics (number of droplets with nuclei in a given time interval) for a population of droplets of ~140 μm initial size. Droplets shrink rapidly in <10 s, followed by nucleation events in individual drops. (b) Statistical analysis of nucleation induction time measurements for the same sample: the horizontal axis shows the time after dispensing (t), while the vertical axis corresponds to the natural logarithm of the probability (P) of no nucleation in a drop within a time t (as obtained from the five different ensembles of drops, with a total of 415 nucleation events observed). A compressed exponential model $P = \exp[(-t/\tau)^{\beta}]$ was fitted to the data with an R^2 value of 0.99, an average induction time τ of 102 s, and a compressed exponent β of 2.02.

Poisson process with a *time-dependent* rate parameter $\lambda(t) \sim t/\tau^2$, which increases with time.[24]

We interpret these results by commenting on the possible mechanisms of nucleation within drops. We can effectively rule out heterogeneous nucleation by *external* impurities such as dust particles, because the likely number of impurities is significantly smaller than the number of droplets in an emulsion-based system.[25] Moreover, we observed that in the rare cases where a visible impurity was present in a droplet — a fibrous dust particle for example — large, faceted α-glycine crystals were obtained. If each drop is assumed to be isolated from the influence of other drops in the ensemble, then two mechanistic candidates remain for our consideration: (i) homogeneous nucleation within the drops and (ii) heterogeneous nucleation at the oil–water interface (aided by surfactants or otherwise), which has been documented in several reports of crystallization in emulsions.[3,22,26] While we cannot rule out either mechanism, we note that both can be modeled by homogeneous Poisson processes, albeit with different time constants. However, our attempts to fit the data with simple two-exponential models[27] were unsuccessful. On the other hand, we could accurately describe the process with a compressed exponential model, as stated above. This model highlights an important fact about our experimental system — that the drops on the heated slide are not necessarily isolated from the influence of events in surrounding drops. The

dx.doi.org/10.1021/cg300413s | *Cryst. Growth Des.* 2012, 12, 3977–3982

increasing rate parameter of the compressed exponential model likewise suggests that the presence of formed SAs increases the likelihood of nucleation in the uncrystallized droplets. As an extreme example of this phenomenon, we have observed that formed SAs can trigger nucleation within droplets in their immediate vicinity (a sample image sequence is provided in the Supporting Information). Further detailed measurements and more quantitative analyses of nucleation statistics within such crystallizing droplet ensembles are ongoing and will be the topic of a forthcoming report.

Next, high-speed stereomicroscopic visualization at the single-droplet scale provided insights into the physics of crystal growth. Nucleation typically occurred at a random location within or at the surface of a droplet, and crystal growth occurred rapidly from the nucleus along radially advancing fronts at speeds of ∼1 mm/s. We conducted digital image analyses of crystal growth within the droplets (details of the procedure are provided as Supporting Information), by measuring the radial interface position from the nucleation site (r) for several directions versus time (t). Digital micrographs captured at high imaging speeds and image analysis results are provided in Figure 6 for selected typical

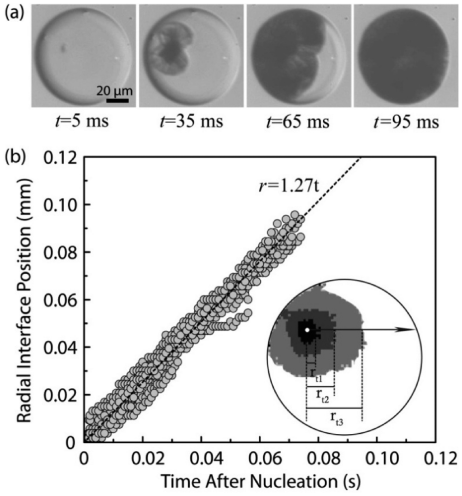

Figure 6. Growth of spherical agglomerates after the nucleation event: (a) high-speed microscopic images of a growing SA obtained at the flow rate combination Q_{CP} = 1000 μL/min, Q_{DP} = 20 μL/min, (b) the evolution of a 110 μm SA after the nucleation event. It can be seen that radial crystal growth, measured as the position of the interface versus time, assumes a distinctly linear profile (with crystallization speeds of ∼1.3 mm/s), a characteristic of spherulitic crystallization. The inset shows an example of how crystal growth is measured via digital image analysis: the radial interface position is tracked along a variety of directions from the point of nucleation; a sample direction is indicated.

cases. Interestingly, we observed linear crystal growth (i.e., $r \propto t$) in all cases, strongly suggesting a spherulitic growth mechanism observed commonly in impure melts, where crystal growth is faster than diffusive mass transfer.[28,29] Simple estimates of glycine concentrations within the droplets support the hypothesis that conditions within the emulsion droplets after shrinkage are conducive to a spherulitic growth mechanism. Assuming a uniform temperature of 84 °C, droplet shrinkage of ∼50% and no glycine leaving the droplets, we estimate that supersaturation values within the shrunk droplets range between 3.5 and 6.5 (for the range of drop sizes used in this study), with dissolved glycine concentrations of 18.6−20.0 kmol/m^3 and water concentrations of ∼0.3 kmol/m^3. These values correspond to glycine concentrations of 1.3−1.5 g/mL, which are very close to the solid density of glycine (∼1.6 g/mL). Moreover, drastic decreases in mutual diffusivities have been reported for supersaturated aqueous glycine solutions, with very low ($\ll 10^{-9}$ m^2/s) values above supersaturations of ∼1.5.[30] Given these facts, it is plausible that the contents within the droplets resemble impure *melts*, with water acting as the impurity, in which the spherulitic crystal growth mechanism has been well documented.[28] Further, extremely low molecular diffusivities at high supersaturation could also account for the observation of rapid initial shrinkage of droplets followed by a prolonged stagnation of their sizes. Finally, once formed, most agglomerates go through an aging process which is typically completed within ∼3−10 s of crystallization and leads to a coarser surface, likely due to phase transformation and Ostwald ripening mediated by trapped water within the agglomerate.[31] A typical series of microscope images showing the observable coarsening of an agglomerate is provided in the Supporting Information. A detailed investigation of the exact nature of the aging phenomenon is under way.

■ CONCLUDING REMARKS

Our studies involve a "canonical" model API molecule, that is, glycine, which is commonly employed in developing new polymorphic crystallization strategies. Our ongoing work is focused along two primary directions: (i) toward detailed understanding of such (previously unreported) crystallization phenomena within microscale emulsion drops, and (ii) toward continuous, scalable processing. Further understanding of crystallization *dynamics*, using a coupled experimental and theoretical approach, is crucial to establish the extent to which conclusions based on glycine can be generalized to similar molecules (such as charged zwitterionic amino acids) and also to a broader range of API molecule types. Crystallization and aging dynamics, in conjunction with the preponderance of fluid−fluid interfaces, also likely dictates the polymorphic outcome of the spherical crystallization process. To probe this further, we are currently investigating the effect of several parameters such as temperature, droplet size, dissolved additives, etc. on the outcome of the crystallization process.[32] Second, our method involves emulsion generation and subsequent evaporative crystallization in static fashion on a heated platform. Therefore, the overall method is *semibatch* in nature. Scalability of emulsion generation, especially in the context of low-volume high-value pharmaceuticals, can be achieved by modest parallelization of the microfluidic emulsion generators. The design and configuration of fully *continuous* processing units will involve parallelized emulsion generators coupled in series with downstream units that create supersaturation in the generated emulsions either by the vacuum or by heating. The design and optimization of such units will involve straightforward application of the above fundamental studies in dynamics and is the subject of ongoing work. In conclusion, we have demonstrated spherical glycine crystallization in monodisperse emulsions generated using a simple capillary-based microfluidic device. Spherical glycine crystal agglomerates are produced with a remarkable level of control over shape, size, and size-distribution. Our studies also shed light on the various operative phenomena during crystallization and raise interesting and fundamental questions. This work

paves the way for microfluidics-enabled continuous spherical crystallization processes.

■ ASSOCIATED CONTENT

Supporting Information

I. Assembly and exact specifications of the microfluidic devices used. II. Images of droplet breakup at different flow rate combinations. III. Details of the image analysis. IV. Observational evidence for SA-triggered nucleation. V. Microscopic observation of the aging phenomenon. This information is available free of charge via the Internet at http://pubs.acs.org/.

■ AUTHOR INFORMATION

Corresponding Author

*E-mail: chesakk@nus.edu.sg.

Notes

The authors declare no competing financial interest.

■ ACKNOWLEDGMENTS

The authors gratefully acknowledge research funding from the GSK-EDB Fund for Sustainable Manufacturing in Singapore and the Chemical and Pharmaceutical Engineering Programme of the Singapore-MIT Alliance.

■ ABBREVIATIONS

API: active pharmaceutical ingredient; CP: continuous phase; d: diameter; D_A: average agglomerate diameter; DP: dispersed phase; D_D: droplet diameter; FE-SEM: field emission scanning electron microscopy; ID: inner diameter; OD: outer diameter; P: probability of no nucleation event at a given time; Q_{CP}: volumetric flow rate of continuous phase (dodecane); Q_{DP}: volumetric flow rate of dispersed phase (aqueous glycine); r: radial interfacial position of forming spherical agglomerate; SA: spherical agglomerate; std. dev.: standard deviation; t: time elapsed after nucleation in an individual agglomerate; t': time elapsed after dispensing droplets on the glass slide; τ: average induction time; PXRD: powder X-ray diffraction

■ REFERENCES

(1) Variankaval, N.; Cote, A. S.; Doherty, M. F. *AIChE J.* **2008**, *54*, 1682−1688.
(2) Kawashima, Y.; Okumura, M.; Takenaka, H. *Science* **1982**, *216*, 1127−1128.
(3) Chadwick, K.; Davey, R. J.; Mughal, R.; Marziano, I. *Org. Process Res. Dev.* **2009**, *13*, 1284−1290.
(4) Nocent, M.; Bertocchi, L.; Espitalier, F.; Baron, M.; Couarraze, G. *J. Pharm. Sci.* **2001**, *90*, 1620−1627.
(5) Christopher, G. F.; Anna, S. L. *J. Phys. D: Appl. Phys.* **2007**, *40*, R319−R336.
(6) Wang, J. T.; Wang, J.; Han, J. J. *Small* **2011**, *7*, 1728−1754.
(7) Zhu, L.; Li, Y.; Zhang, Q.; Wang, H.; Zhu, M. *Biomed. Microdevices* **2010**, *12*, 169−177.
(8) Shum, H. C.; Kim, J. W.; Weitz, D. A. *J. Am. Chem. Soc.* **2008**, *130*, 9543−9549.
(9) Shah, R. K.; Kim, J. W.; Weitz, D. A. *Adv. Mater.* **2009**, *21*, 1949−1953.
(10) Edd, J. F.; Humphry, K. J.; Irimia, D.; Weitz, D. A.; Toner, M. *Lab Chip* **2009**, *9*, 1859−1865.
(11) Stan, C. A.; Schneider, G. F.; Shevkoplyas, S. S.; Hashimoto, M.; Ibanescu, M.; Wiley, B. J.; et al. *Lab Chip* **2009**, *9*, 2293−2305.
(12) Morissette, S. L.; Almarsson, O.; Peterson, M. L.; Remenar, J. F.; Read, M. J.; Lemmo, A. V.; et al. *Adv. Drug Delivery Rev.* **2004**, *56*, 275−300.
(13) Hansen, C. L. *Proc. Natl. Acad. Sci. U. S. A.* **2002**, *99*, 16531−16536.
(14) Zheng, B.; Roach, L. S.; Ismagilov, R. F. *J. Am. Chem. Soc.* **2003**, *125*, 11170−11171.
(15) Shim, J. U.; Cristobal, G.; Link, D. R.; Thorsen, T.; Jia, Y.; Piattelli, K.; et al. *J. Am. Chem. Soc.* **2007**, *129*, 8825−8835.
(16) He, G.; Bhamidi, V.; Tan, R. B. H.; Kenis, P. J. A.; Zukoski, C. F. *Cryst. Growth Des.* **2006**, *6*, 1175−1180.
(17) Teychené, S.; Biscans, B. *Cryst. Growth Des.* **2011**, *11*, 4810−4818.
(18) Thiele, J.; Windbergs, M.; Abate, A. R.; Trebbin, M.; Shum, H. C.; Förster, S.; et al. *Lab Chip* **2011**, *11*, 2362−2368.
(19) Tanaka, M.; Yamanaka, S.; Shirakawa, Y.; Shimosaka, A.; Hidaka, J. *Adv. Powder Technol.* **2011**, *22*, 125−130.
(20) Steinbacher, J. L.; Moy, R. W. Y.; Price, K. E.; Cummings, M. A.; Roychowdhury, C.; Buffy, J. J.; et al. *J. Am. Chem. Soc.* **2006**, *128*, 9442−9447.
(21) Utada, A.; Chu, L.; Fernandez-Nieves, A.; Link, D.; Holtze, C.; Weitz, D. *MRS Bull.* **2007**, *32*, 702−708.
(22) Allen, K.; Davey, R. J.; Ferrari, E.; Towler, C.; Tiddy, G. J.; Jones, M. O.; et al. *Cryst. Growth Des.* **2002**, *2*, 523−527.
(23) Poornachary, S. K.; Chow, P. S.; Tan, R. B. H. *Cryst. Growth Des.* **2008**, *8*, 179−185.
(24) Ross, S. M. *Simulation*; Elsevier Academic Press: Waltham, MA, 2006; p 32.
(25) Davey, R. J.; Garside, J.; Hilton, A. M.; McEwan, D.; Morrison, J. W. *Nature* **1995**, *375*, 664−666.
(26) Chen, C.; Cook, O.; Nicholson, C. E.; Cooper, S. J. *Cryst. Growth Des.* **2011**, *11*, 2228−2237.
(27) Laval, P.; Crombez, A.; Salmon, J. B. *Langmuir* **2009**, *25*, 1836−1841.
(28) Keith, H. D.; Padden, F. J. *J. Appl. Phys.* **1963**, *34*, 2409−2421.
(29) Goldenfeld, N. *J. Cryst. Growth* **1987**, *84*, 601−608.
(30) Chang, Y. C.; Myerson, A. S. *AIChE J.* **1986**, *32*, 1567−1569.
(31) Cardew, P. T.; Davey, R. J. *Proc. R. Soc. London A* **1985**, *398*, 415−428.
(32) Diao, Y.; Whaley, K. E.; Helgeson, M. E.; Woldeyes, M. A.; Doyle, P. S.; Myerson, A. S.; et al. *J. Am. Chem. Soc.* **2012**, *134*, 673−684.